SECONDARY GAMMA-RAY PRODUCTION IN A CODED APERTURE MASK.

A. Owens, G.M. Frye, Jr., C.J. Hall, T.L. Jenkins, G.N. Pendleton.
Case Western Reserve University, Cleveland Ohio 44106, U.S.A.

J.N. Carter, D. Ramsden,
Southampton University, Southampton SO9 5NH, U.K.

B. Agrinier, E. Bonfand, C. Gouiffes, A. Tabary,
Section d'Astrophysique, Centre d'Etudes Nucleâires de Saclay, France.

1. Introduction. The application of the coded aperture mask to high energy γ-ray astronomy will provide the capability of locating a cosmic γ-ray point source with a precision of a few arc-minutes above 20 MeV (1). Recent tests using a mask in conjunction with drift chamber detectors have shown that the expected point spread function is achieved over an acceptance cone of 25^0 (2). A telescope employing this technique differs from a conventional telescope only in that the presence of the mask modifies the radiation field in the vicinity of the detection plane. In addition to reducing the primary photon flux incident on the detector by absorption in the mask elements, the mask will also be a secondary radiator of γ-rays. In this paper we consider the various background components in a CAMTRAC (Coded Aperture Mask Track Chamber) telescope and compare Monte-Carlo calculations with recent measurements obtained using a prototype instrument in a tagged photon beam line. This instrument is described elsewhere in this conference (3).

2. Secondary Background Production in a Mask. There are several mechanisims by which photons may be generated in a mask. Charged particles may generate γ-rays via bremsstralung, π^0-production or spallation in the mask material. By using veto counters, in front of and behind the mask, it is estimated that the contribution due to these components will be $< 10^{-5}$ γ's per incident particle, and therefore they can be neglected. Neutron interactions in the mask may produce secondary γ's through neutron capture or inelastic scattering. Butler et al. (4) have shown that this component is negligible, being $< 10^{-6}$ γ's per incident neutron for photon energies above 10 MeV. Gamma-rays incident on a mask may Compton scatter, or produce pairs within the mask material, that generate secondary photons by bremsstralung of the first generation electron(s), or (if an electromagnetic cascade is induced) by the secondary electrons. This component is potentially the most troublesome since in some of these

interactions none of the electrons will reach the veto counters.

3. Monte-Carlo Calculations. Monte-Carlo calculations have been carried out using the EGS electron-photon transport code of Ford and Nelson (5). Mono-energetic photons were allowed to fall normally on lead slabs of various thicknesses and the secondary photon and electron energy and radial distributions recorded. These distributions were found to agree, within statistical uncertainty, with those derived using the calculations of Messel and Crawford (6) and the experimental data of Darriulat et al. (7) In Fig. 1 we consider the various components that emerged from a 2.73 RL tungsten slab as a function of incident photon energy. A secondary photon threshold of 12.5 MeV was assumed in the calculations, this value being representative of the lower limit of our telescope. The various contributions arise as follows; F_1 is the transmitted component (i.e. $F_1 = e^{-\mu(E)t}$ where $\mu(E)$ is the linear attenuation coefficient of the mask material and t is the mask thickness), F_2 is the fraction of incident photons that generated secondary γ-rays, F_3 is the fraction of incident photons in which secondary γ-rays were also accompanied by an electron with a kinetic energy > 1 MeV, and F_4 is the fraction of incident photons that produced secondary γ-rays and no electron > 1 MeV that left the slab. Therefore $F_2 = F_3 + F_4$. A scintillation counter placed immediately behind the slab will veto component F_3, and thus F_4 represents the intrinsic secondary background due to the mask. The energy spectrum of the unvetoed secondary component, integrated over 2π steradians, was found to be well represented by the empirical function;

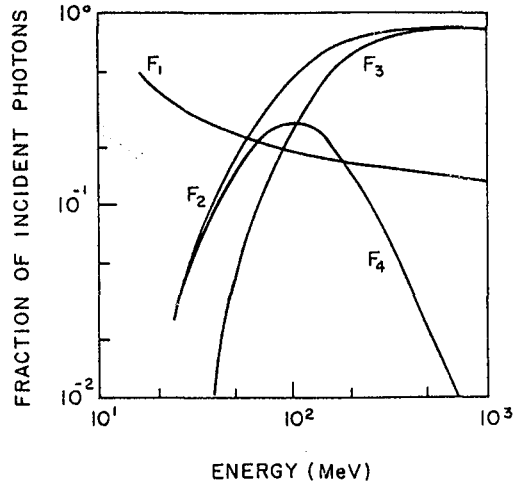

Fig. 1 The fraction of the various classes of events emitted from a 2.73 RL tungsten slab as a function of incident photon energy. Refer to the text for the definition of the symbols used.

$$dN(E,\bar{E}) = 3.79 \times 10^{-2}\, E^{0.96}\, \bar{E}^{-a}\, \exp(-1.054 \times 10^{-2} E) \times \exp(-47.17\, \bar{E}\, E^{-1.55})\, d\bar{E} \quad \gamma\text{'s / incident photon MeV} \qquad (1)$$

where $a = \begin{cases} 0.843 + 3.6 \times 10^{-3} E - 6.3 \times 10^{-6} E^2, & 20 \leq E \leq 400 \text{ MeV} \\ 1.29, & E > 400 \text{ MeV} \end{cases}$

and E and $\bar{E}$ are the incident and secondary γ-ray energies respectively. By comparison with Monte-Carlo data it is estimated that the average error in $dN(E,\bar{E})$, determined by Eq. 1, is < 10% over the incident energy range 20 to 600 MeV and secondary energies $1 < \bar{E} < E$.

In Fig. 2 we consider the case for a spectrum varying as E^{-2} normally incident on a mask consisting of equal open and opaque elements. The various components are shown separately integrated over 2π steradians. The band in the Fig. encompasses single and multiple secondary photon emission. For any detection system placed immediately behind the mask the true detector background would lie within these bounds. It can be seen from Fig. 2 that the unvetoed secondary component constitutes < 5% of the incident γ-rays. Further, since this component drops more rapidly than the incident flux ($\sim E^{-3}$ as opposed to E^{-2}) it can be neglected for energies > 200 MeV. It should be noted that for a practical telescope with a mask and a detection area of 1 m^2, separated by 1 m, the measured unvetoed background will be approximately a factor of 1.2 lower than that shown at energies < 20 MeV due to the angular distribution of the secondary γ-rays. The median of this distribution ranges from about 15° to 3° for secondary energies 10 MeV to 200 MeV. Since this is much greater than the angular size of the unit mask cell at the detection plane, the secondary γ-rays will not reproduce the mask pattern, and will therefore constitute an almost uniform background level.

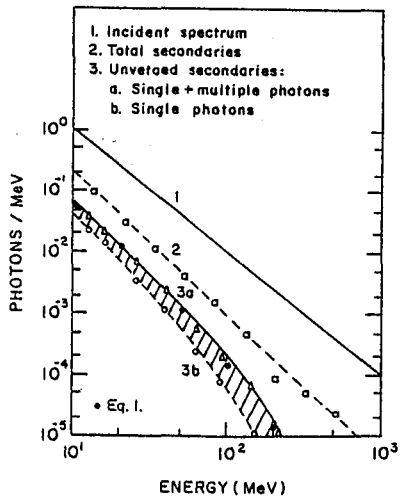

Fig. 2 The various contributions to a detector counting rate for an E^{-2} spectrum normally incident on a tunsten mask of thickness 2.73 RL.

4. Experimental. It can be seen from Fig. 1 that the most efficient production of unvetoed secondary photons occurs for incident γ-ray energies of $\sim$100 MeV. For this reason secondary γ-ray spectra have been measured at a range of incident photon energies ranging from 23 to 400 MeV using a CAMTRAC telescope at the tagged photon facility at CEN Saclay,

France. Here we report preliminary results for normally incident γ-rays of energies 27, 48, 90 and 108 MeV. The mask used during these runs was a 2.73 RL tungsten checkerboard of unit cell size 6.3 mm. A counter in front of the mask vetoed charged particle induced events, while a counter behind the mask tagged those events in which a secondary γ-ray was also accompanied by a charged particle that did not trigger the detector anti-coincidence. A calorimeter located behind the track chamber measured the photon energy with a typical energy resolution of 57% FWHM at 100 MeV. Fig. 3 shows the total secondary spectra measured at various incident energies. These were determined by comparing runs with and without the mask in place. For comparison the results of Monte-Carlo calculations are also shown from which it can be seen there is reasonable agreement. Also shown in Fig. 3 is the spectrum of events for which a charged particle (> 1 MeV) was also detected in the counter behind the mask, from which we conclude that the unvetoed secondary component produced in the mask comprises at worst $\sim 10^{-3}$ γ's per incident photon per MeV.

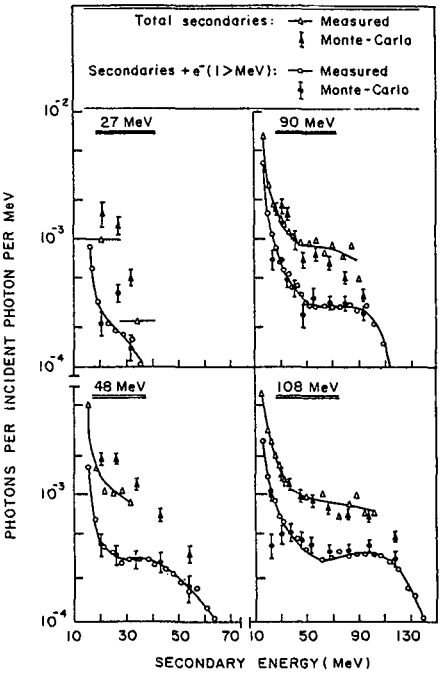

Fig. 3 Experimental and Monte-Carlo secondary γ-ray spectra at various incident γ-ray energies.

5. Acknowledgements. This work was supported by NASA grant NAGW-451 and grants from the SERC.

References

1. Carter, J.N. et al; Mon. Not. R. Astr. Soc., 198 (1982) 33.
2. Frye, G.M., Jr., et al; to be published in the Proc. of the Workshop on the Space Station, LSU (1984).
3. Jenkins, T.L. et al; this conference, paper OG 9.2-7.
4. Butler, R.C. et al; Nucl. Instr. and Meth., 221 (1984) 41.
5. Ford, R.L. and Nelson, W.R.; The EGS code system, SLAC-210 (1978).
6. Messel, H. and Crawford, D.F.; Electron-Photon Shower Distribution Function Tables for Lead, Copper and Air absorbers, Pergamon Press New York (1970).
7. Darriulat, P. et al; Nucl. Instr. and Meth., 129 (1975) 105.